Intrinsically disordered protein regions are required for cell wall homeostasis in *Bacillus subtilis*

Yannick R. Brunet, Cameron Habib, Anna P. Brogan, Lior Artzi, and David Z. Rudner

Department of Microbiology, Harvard Medical School, Boston, Massachusetts 02115, USA

Intrinsically disordered protein regions (IDRs) have been implicated in diverse nuclear and cytoplasmic functions in eukaryotes, but their roles in bacteria are less clear. Here, we report that extracytoplasmic IDRs in *Bacillus subtilis* are required for cell wall homeostasis. The *B. subtilis* σ^I transcription factor is activated in response to envelope stress through regulated intramembrane proteolysis (RIP) of its membrane-anchored anti-σ factor, RsgI. Unlike canonical RIP pathways, we show that ectodomain (site-1) cleavage of RsgI is constitutive, but the two cleavage products remain stably associated, preventing intramembrane (site-2) proteolysis. The regulated step in this pathway is their dissociation, which is triggered by impaired cell wall synthesis and requires RsgI's extracytoplasmic IDR. Intriguingly, the major peptidoglycan polymerase PBP1 also contains an extracytoplasmic IDR, and we show that this region is important for its function. Disparate IDRs can replace the native IDRs on both RsgI and PBP1, arguing that these unstructured regions function similarly. Our data support a model in which the RsgI–σ^I signaling system and PBP1 represent complementary pathways to repair gaps in the PG meshwork. The IDR on RsgI senses these gaps and activates σ^I, while the IDR on PBP1 directs the synthase to these sites to fortify them.

[*Keywords*: peptidoglycan; class A PBP; regulated intramembrane proteolysis (RIP); intrinsically disordered protein region; mechanotransduction; Notch; aGPCR]

Supplemental material is available for this article.

Received July 11, 2022; revised version accepted October 3, 2022.

Intrinsically disordered proteins (IDPs) and protein regions (IDRs) have been implicated in diverse cellular processes in eukaryotes, including differentiation, transcription, pre-mRNA processing, DNA condensation, and signal transduction (Oldfield and Dunker 2014). In most cases, these regions are intracellular and function as interaction hubs in multiprotein networks (Wright and Dyson 2015). Some of these IDPs and IDRs have also been shown to promote the formation of membraneless organelles via liquid–liquid phase separation and have been associated with neurodegeneration and cancer (Boeynaems et al. 2018). In contrast, the functions of IDRs in bacteria are less clear. A few IDRs have been found to serve as cytoplasmic interaction hubs, including regions found on the cell division protein FtsZ and the polar organizer PopZ (Gardner et al. 2013; Buske et al. 2015; Du et al. 2015; Holmes et al. 2016). Similarly, some IDRs, like the intrinsically disordered linker on the single-strand DNA-binding protein SSB, have been shown to promote phase-separated condensates (Harami et al. 2020; Lasker et al. 2020; Azaldegui et al. 2021). Here, we provide evidence for a new role for bacterial IDRs that are present on broadly conserved proteins involved in cell wall biogenesis: sensing and responding to defects in the cell wall.

The cell wall peptidoglycan (PG) specifies cell shape and protects bacteria from osmotic lysis, and its synthesis is the target for some of the most successful antibiotics (Typas et al. 2012; Rohs and Bernhardt 2021). It is a covalently closed macromolecule composed of long glycan strands cross-linked together by short peptide bridges. Two types of PG synthases are responsible for the assembly of this essential exoskeleton (Rohs and Bernhardt 2021). Class A PBPs (aPBPs) are bifunctional enzymes that contain glycosyltransferase (GT) domains that polymerize glycan strands and transpeptidase (TP) domains that cross-link them into the PG meshwork (Goffin and Ghuysen 1998). SEDS proteins are glycan strand polymerases that work with cognate class B PBPs (bPBPs) that have peptide cross-linking activity (Meeske et al. 2016; Taguchi et al. 2019; Sjodt et al. 2020). Evidence suggests that in rod-shaped bacteria, the SEDS polymerase RodA and its cognate, bPBP, synthesize foundational glycan strands in the

Corresponding author: rudner@hms.harvard.edu
Article published online ahead of print. Article and publication date are online at http://www.genesdev.org/cgi/doi/10.1101/gad.349895.122.

context of multimeric membrane complexes called the Rod complex, while the aPBPs act semiautonomously to fortify the wall and repair or fill gaps (Cho et al. 2016; Lai et al. 2017). In Gram-negative bacteria, outer membrane-localized Lpo factors are essential for the PG synthesis activity of aPBPs (Paradis-Bleau et al. 2010; Typas et al. 2010). These Lpo factors interact with their cognate inner membrane-localized aPBPs across the cell wall meshwork that separates them. Accordingly, this *trans*-PG interaction targets aPBP synthesis to gaps or pores in the meshwork, enabling their fortification (Typas et al. 2012; Vigouroux et al. 2020; Rohs and Bernhardt 2021). No equivalent system has been identified in Gram-positive bacteria that have a thicker multilayered cell wall and lack an outer membrane.

Expansion of the PG meshwork during growth also requires cell wall hydrolases that cleave bonds in the meshwork to allow insertion of new material (Weidel and Pelzer 1964; Doyle and Koch 1987; Uehara and Bernhardt 2011; Rohs and Bernhardt 2021). How cells monitor PG biogenesis and make adjustments to its synthesis and/or hydrolysis remains poorly understood. We recently reported that the broadly conserved WalR–WalK two-component signaling system in *B. subtilis* modulates the levels and activities of two PG hydrolases (LytE and CwlO) that are required for cell wall expansion during growth by monitoring the extent of cell wall hydrolysis (Dobihal et al. 2019). Here, we describe a second cell envelope homeostatic pathway that responds to defects in the cell wall meshwork and involves the alternative σ factor σ^I and its membrane-anchored anti-σ factor, RsgI.

σ^I was originally identified as a heat-shock σ factor (Zuber et al. 2001; Asai et al. 2007); however, most of its validated targets are genes involved in cell wall biogenesis (Tseng and Shaw 2008; Tseng et al. 2011; Salzberg et al. 2013), suggesting that the RsgI–σ^I pathway senses and responds to envelope stress. In support of this idea, σ^I-dependent transcription was recently shown to increase in the absence of aPBPs, and aPBP-deficient cells require σ^I for viability (Patel et al. 2020). What this pathway senses remains unknown. However, evidence suggests that the signal transduction pathway that activates σ^I involves regulated intramembrane proteolysis (RIP) of the RsgI anti-σ factor (Liu et al. 2017; Patel et al. 2020). RIP signaling pathways in bacteria control extracytoplasmic function (ECF) σ factors through the regulated intramembrane cleavage of their membrane-anchored anti-σ factors (Ho and Ellermeier 2012; Schneider and Glickman 2013). In these pathways, a so-called site-1 protease (S1P) cleaves and releases the extracytoplasmic domain of the anti-σ factor. Removal of the ectodomain allows cleavage by a site-2 protease of the S2P/RseP family. These membrane-embedded metalloproteases cleave their substrate within or adjacent to the lipid bilayer and release the cytoplasmic anti-σ factor domain, which is further degraded, liberating the active transcription factor. S2P/RseP family members have extracytoplasmic PDZ domains, and analysis of *E. coli* RseP indicates that these domains function as size exclusion filters, preventing substrates with intact ectodomains from accessing the recessed catalytic center of the membrane protease (Hizukuri et al. 2014; Akiyama et al. 2015). Thus, in all characterized examples, the regulated step in RIP signaling pathways is site-1 proteolysis (Kroos and Akiyama 2013).

Here, we report that, unlike canonical RIP pathways, site-1 cleavage of RsgI is constitutive, but the two cleavage products remain stably associated, preventing intramembrane proteolysis. In response to envelope stress, the cleavage products dissociate, triggering S2P proteolysis and σ^I activation. Importantly, RsgI has an extracytoplasmic IDR, and we demonstrate that this region is required to activate σ^I in response to impaired cell wall synthesis and is likely responsible for generating the force that pulls the site-1-cleaved products apart. Intriguingly, the major aPBP in *B. subtilis* (PBP1) and its homologs in Gram-positive bacteria also contain extracytoplasmic IDRs, and we show that this region is important for PBP1 function. We further demonstrate that disparate IDRs from PBP1 and RsgI homologs can replace the native IDRs on both *B. subtilis* proteins, suggesting that these regions function similarly. Finally, we show that both RsgI and PBP1 retain full function when the order of the amino acids in their native IDRs is scrambled, indicating that disorder itself is central to their activity. Collectively, our data support a model in which the IDR on RsgI senses gaps in the cell wall matrix and activates σ^I through mechanotransduction to promote their repair, while the IDR on PBP1 functions like the Lpo factors in Gram-negative bacteria, localizing the PG synthase to these same sites to fortify them.

Results

The RsgI–σ^I pathway is involved in homeostatic control of PG biogenesis

In *B. subtilis*, the cell wall hydrolases LytE and CwlO are required for cell wall elongation (Bisicchia et al. 2007; Hashimoto et al. 2012). To identify factors that regulate LytE, we performed a synthetic lethal screen taking advantage of the fact that LytE and CwlO are functionally redundant and essential for growth. We used transposon sequencing (Tn-seq) to screen for genes that could tolerate Tn insertions in wild type but not in a Δ*cwlO* mutant and identified *lytE*, *sigI*, *rasP*, *ecsA*, and *ecsB* (Supplemental Fig. S1). Using a CwlO depletion strain, we confirmed that null mutations in all five genes were synthetic lethal with Δ*cwlO* (Supplemental Fig. S2A). The product of *sigI*, σ^I, was previously shown to regulate *lytE* transcription (Tseng et al. 2011) and have a synthetic lethal relationship with CwlO (Salzberg et al. 2013). RasP is the *B. subtilis* site-2 protease of the S2P/RseP family, and recent work indicates that it is required for σ^I activity (Liu et al. 2017; Patel et al. 2020). Finally, EcsA and EcsB are homologous to ABC transporter complexes and are required for RasP-mediated cleavage of the anti-σ factor RsiW (Heinrich et al. 2008). These findings are consistent with previous studies suggesting that RasP and EcsAB control σ^I-dependent transcription of *lytE* through regulated intramembrane proteolysis (RIP) of the anti-σ^I factor RsgI (Liu et al. 2017; Patel et al. 2020). In support of this model, deletion

of *rsgI*, resulting in constitutive σ^I activity, suppressed the synthetic lethality of Δ*cwlO*Δ*rasP* and Δ*cwlO*Δ*ecsAB* but not Δ*cwlO*Δ*sigI* or Δ*cwlO*Δ*lytE* (Supplemental Fig. S2B).

Analysis of LytE levels and σ^I activity provides further support for RIP signaling. As can be seen in Figure 1A, LytE levels were reduced in exponentially growing cells lacking σ^I, RasP, or EcsA. Furthermore, using the σ^I-responsive promoter of the *bcrC* gene fused to *lacZ* (Supplemental Fig. S3; Tseng and Shaw 2008), we found that σ^I activity was reduced in cells lacking RasP and EcsA and strongly increased in the absence of the anti-σ^I factor RsgI (Fig. 1B).

σ^I was originally identified as a heat-shock σ factor (Zuber et al. 2001; Asai et al. 2007); however, most of its targets are involved in cell wall biogenesis (Tseng and Shaw 2008; Tseng et al. 2011; Salzberg et al. 2013), suggesting that the σ^I–RsgI pathway senses and responds to envelope stress. To gain insight into the signals that activate σ^I, we used Tn-seq to screen for genes that become essential in the absence of *sigI*. In addition to *cwlO* and the genes required for its activity (Supplemental Fig. S4A; Domínguez-Cuevas et al. 2013; Meisner et al. 2013; Brunet et al. 2019), insertions in *ponA* encoding the major class A penicillin-binding protein PBP1 were underrepresented in cells lacking σ^I (Supplemental Fig. S4B). A reciprocal screen aimed at identifying genes that become essential in the absence of this important cell wall synthase identified *sigI* (Supplemental Fig. S4C; Patel et al. 2020). Depletion of PBP1 in the Δ*sigI* mutant confirmed the synthetic lethal relationship (Supplemental Fig. S4E). These findings raised the possibility that cells lacking PBP1 induce σ^I-dependent gene expression, and that was indeed the case (Fig. 1C; Supplemental Fig. S4D; Patel et al. 2020). To investigate whether *B. subtilis* modulates σ^I activity in response to changes in PBP1-mediated cell wall synthesis, we varied PBP1 levels using an IPTG-regulated promoter and monitored σ^I-dependent *lacZ* expression (Fig. 1C). We observed a graded increase in σ^I activity in response to decreasing levels of PBP1. These results support the idea that this RIP signaling pathway functions in the homeostatic control of cell wall biogenesis.

σ^I is regulated by intramembrane proteolysis of RsgI

To investigate whether RsgI is subject to RasP-mediated intramembrane proteolysis, we constructed a GFP-RsgI-His fusion to monitor the N-terminal and C-terminal RsgI cleavage products (Fig. 2A). The fusion maintained σ^I-dependent gene expression at levels that were lower than the native RsgI protein, but the fold induction in the absence of PBP1 was similar to wild type (Supplemental Figs. S3, S5), indicating that GFP-RsgI-His is subject to similar regulatory control. Immunoblot analysis from exponentially growing cells revealed four predominant RsgI species: full-length GFP-RsgI-His, a C-terminal cleavage product recognized by anti-His antibodies, and two N-terminal cleavage products recognized by anti-GFP antibodies (Fig. 2B). In the absence of the RasP site-2 protease, the smaller N-terminal cleavage product was absent, and the levels of the larger N-terminal cleavage product increased (Fig. 2B). These data indicate that RsgI is subject to RasP proteolysis and suggest that the larger N-terminal (GFP-containing) cleavage product and the C-terminal (His-containing) cleavage product are generated by a site-1 protease. Finally, consistent with the increased σ^I activity in cells lacking PBP1 (Fig. 1C), in the Δ*ponA* mutant, the levels of the site-1 cleavage products were reduced, presumably due to increased cleavage by RasP (Fig. 2B). The RasP-dependent cleavage product accumulated to a

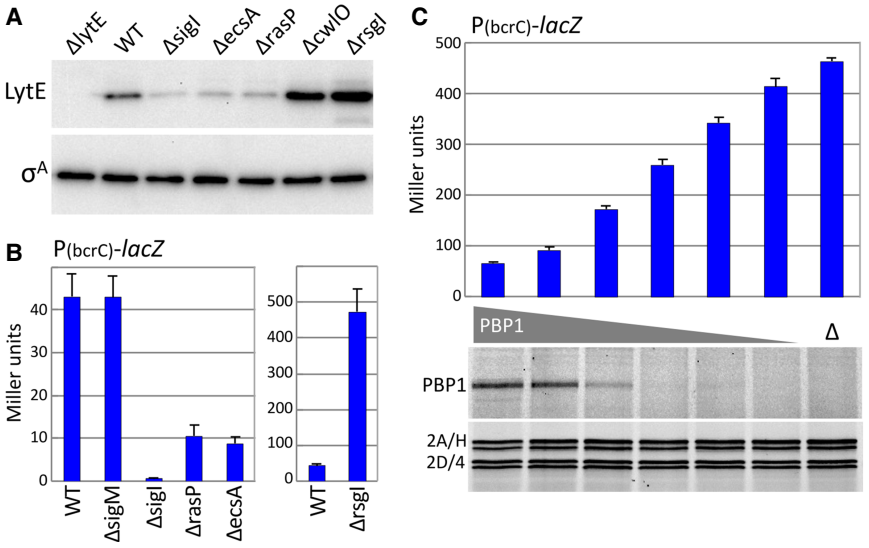

Figure 1. σ^I activity inversely correlates with the level of PBP1. (*A*) Representative immunoblot analysis of LytE in the indicated strains. Midexponential cultures grown in LB were analyzed for the levels of LytE and σ^A to control for loading. (*B*) Bar graph showing β-galactosidase activity in the indicated strains harboring the σ^I-responsive promoter of *bcrC* fused to *lacZ* (P*bcrC-lacZ*). Error bars represent standard deviation from three biological replicates. (*C*) σ^I activity inversely correlates with the level of PBP1. The bar graph shows β-galactosidase activity from the σ^I-responsive reporter in a strain lacking PBP1 (Δ) and strains harboring IPTG-regulated alleles of *ponA*. The first through third lanes, fifth lane, and sixth lane harbor P(IPTG)*-*ponA*. The fourth lane contains P(IPTG)-*ponA*. P(IPTG)* harbors a mutation in the −10 element of P(IPTG), reducing its activity (Griffith and Grossman 2008). β-Galactosidase activity was assayed in exponentially growing cultures in LB supplemented with 250 µM, 125 µM, 50 µM, 0 µM, 25 µM, or no IPTG in the first through sixth lanes, respectively. Error bars represent standard deviation from three biological replicates. PBP1 levels were assessed under the same conditions using bocillin and SDS-PAGE. Labeled proteins were visualized with a Typhoon fluorescence scanner. PBP2A (2A), PBPH (H), PBP2D (2D), and PBP4 (4) are from the same gel and control for loading.

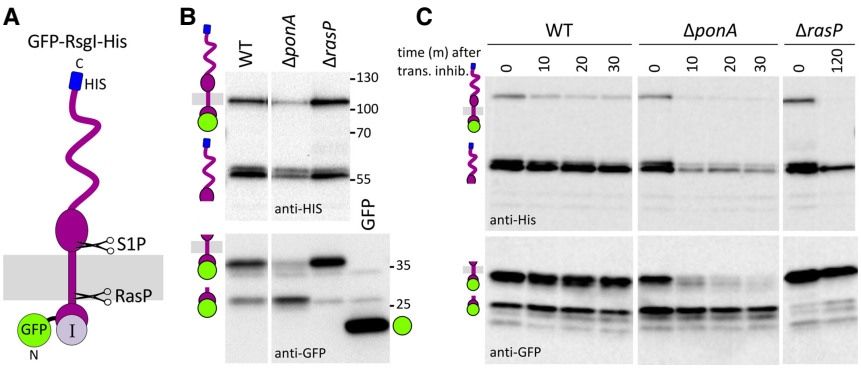

Figure 2. σ^I is regulated by intramembrane proteolysis of RsgI. (*A*) Schematic diagram of the anti-σ^I factor RsgI with GFP and His tags. An unknown site-1 protease (S1P) and the site-2 protease RasP are shown as scissors. (*B*) Representative immunoblot of GFP-RsgI-His in the indicated strains that lack the native *rsgI* gene and harbor a xylose-regulated allele of *gfp-rsgI-his*. All lanes are from the same two blots, with unrelated lanes removed. Schematics show the identity of each band. A strain harboring cytoplasmic GFP (GFP) is included as a size marker. Molecular weight markers are in kilodaltons. (*C*) Immunoblots showing the stability of each GFP-RsgI-His cleavage product in wild type, Δ*ponA*, or Δ*rasP*. Strains were grown in LB medium supplemented with 10 mM xylose to midexponential phase and then treated with spectinomycin and chloramphenicol to inhibit protein synthesis. Samples were collected at the indicated time points (in minutes) before and after inhibition of translation, and GFP-RsgI-His was assessed by immunoblot.

variable degree in this background, and we suspect it is further degraded to release σ^I, as has been reported for the anti-σ^W and anti-σ^V factors RsiW and RsiV (Zellmeier et al. 2006; Liu et al. 2017; Ho and Ellermeier 2019).

Site-1 cleavage of RsgI is constitutive

In virtually all characterized RIP signaling pathways that use RseP/RasP homologs, site-1 proteolysis on the extracytoplasmic side of the membrane is the regulated and rate-limiting step (Kroos and Akiyama 2013). In these cases, the membrane-anchored site-1 cleavage product is only detectable in cells lacking the site-2 protease (Alba et al. 2002; Kanehara et al. 2002; Schöbel et al. 2004; Ellermeier and Losick 2006; Sklar et al. 2010; Hastie et al. 2013). In contrast, RsgI's site-1 cleavage products were readily detectable in wild-type cells (Fig. 2B). To investigate whether these products were transient intermediates, we treated exponentially growing cultures with protein synthesis inhibitors and followed the fate of the cleavage products over time. As can be seen in Figure 2C, the substrate for RasP, the N-terminal membrane-anchored site-1 cleavage product, was stable during the 30-min time course. In contrast, in the Δ*ponA* mutant, this cleavage product was rapidly lost. The extracytoplasmic site-1 cleavage product followed a similar fate: It remained stable in wild type and was rapidly lost in cells lacking PBP1 (Fig. 2C). Furthermore, and as anticipated, depletion of PBP1 in the Δ*rasP* mutant resulted in loss of the extracytoplasmic site-1 cleavage product, while the membrane-anchored site-1 product remained stable (Supplemental Fig. S6). These findings led us to hypothesize that the two site-1 cleavage products stably associate, preventing RasP-mediated site-2 proteolysis, and that the regulated step in this signaling pathway is their dissociation.

The juxtamembrane domain of RsgI is required for ectodomain retention

The extracytoplasmic C terminus of RsgI is composed of two regions (Supplemental Fig. S7): a juxtamembrane domain (~140 amino acids) that is conserved among RsgI homologs and has predicted secondary structural elements (Drozdetskiy et al. 2015; Jumper et al. 2021) and a C-terminal region (~157 amino acids) that is poorly conserved and is predicted to be disordered (Supplemental Figs. S8, S9). To investigate whether the juxtamembrane domain of RsgI is important for the regulation of σ^I activity, we generated amino acid substitutions in six of the most highly conserved residues and analyzed σ^I-dependent *lacZ* expression. In most cases, these mutants resulted in constitutive σ^I activity (Fig. 3A; Supplemental Fig. S10). To analyze the impact on RsgI cleavage, we rebuilt one of these mutations (D95A) in the context of the GFP-RsgI-His fusion. Consistent with constitutive σ^I activity, both site-1 cleavage products in the point mutant failed to accumulate and were rapidly lost upon inhibition of protein synthesis (Fig. 3B). Importantly, in cells lacking RasP, the membrane-anchored site-1 cleavage product was stable, while the C-terminal ectodomain was lost in a manner similar to the RasP$^+$ cells (Fig. 3B). These data are consistent with a model in which the conserved juxtamembrane domain functions to maintain an interaction between the two site-1-cleaved products. Mutations that disrupt this interaction cause ectodomain release, RasP-mediated intramembrane proteolysis, and constitutive σ^I activity.

Stable association between the RsgI site-1 cleavage products

We reasoned that if the N-terminal and C-terminal site-1 cleavage products interact, the soluble extracytoplasmic fragment should remain membrane-associated. To investigate this possibility, we performed fractionation experiments using a strain expressing GFP-RsgI-His. Exponentially growing cells were treated with lysozyme in isotonic buffer to remove the cell wall, and the resulting protoplasts were washed and then lysed in hypotonic buffer. The soluble and membrane-associated proteins were separated by ultracentrifugation and analyzed by immunoblot. As can be seen in Figure 4A, the soluble extracytoplasmic RsgI cleavage product was present in the

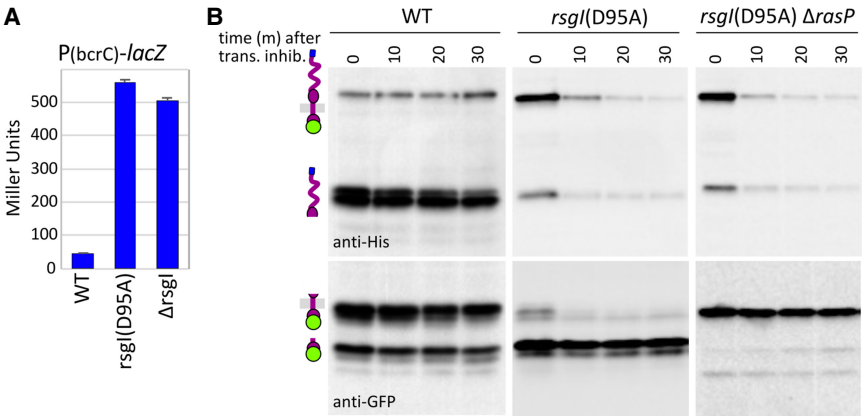

Figure 3. The juxtamembrane domain of RsgI is required for ectodomain retention. (*A*) Bar graph showing β-galactosidase activity from the σ^I-responsive P(bcrC)-*lacZ* reporter in the indicated strains. Activity was assayed in exponentially growing cultures in LB. Error bars represent standard deviation from three biological replicates. (*B*) Representative immunoblots showing the stability of GFP-RsgI-His cleavage products in the indicated strains that lack the native *rsgI* gene and harbor a xylose-regulated allele of *gfp-rsgI-his*. Cells were grown in LB medium supplemented with 10 mM xylose to midexponential phase and then treated with spectinomycin and chloramphenicol to inhibit protein synthesis. Samples were collected at the indicated time points (in minutes) before and after addition of antibiotics, and GFP-RsgI-His was assessed by immunoblot using anti-His and anti-GFP antibodies.

protoplast lysate (lysate), indicating that it remained cell-associated after removal of the cell wall. Furthermore, the majority of this soluble cleavage product fractionated with the membranes (Fig. 4A). A similar fractionation pattern was observed for full-length GFP-RsgI-His, the N-terminal site-1 cleavage product, and a control membrane protein, EzrA (Fig. 4A; Levin et al. 1999). In contrast, the site-2 cleavage product and a control cytoplasmic protein, ScpB (Soppa et al. 2002), were present in the soluble fraction. Importantly, all the proteins and cleavage products that fractionated with the membranes were solubilized in the presence of the nonionic detergent Triton X-100 (Fig. 4A), arguing that their presence in this fraction was not due to aggregation. These data are consistent with the idea that the N-terminal and C-terminal site-1 cleavage products remain stably associated.

To more directly test this model, we purified the soluble C-terminal cleavage product from detergent-solubilized membranes using Ni^{2+} agarose. The immunoblots in Figure 4B show that the eluate contained the C-terminal His-tagged cleavage product in addition to the membrane-anchored N-terminal cleavage product. Analysis of the eluates from an independent purification by SDS-PAGE followed by silver staining (Fig. 4C) revealed two proteins that were specific to the GFP-RsgI-His lysate. These proteins had molecular weights similar to those of the site-1 cleavage products, and mass spectrometry confirmed that the larger was the C-terminal His-tagged cleavage product, while the smaller was the membrane-anchored N-terminal GFP-tagged cleavage product. Similar results were obtained by coimmunoprecipitation using anti-His antibody resin (Supplemental Fig. S11). These data argue that the site-1 cleavage products stably associate, preventing RasP-mediated site-2 proteolysis.

The intrinsically disordered region on RsgI is required to regulate intramembrane proteolysis

We next turned our attention to how the site-1 cleavage products are pulled apart to activate σ^I. The C-terminal region of RsgI is poorly conserved among RsgI homologs but in all cases is predicted to be intrinsically disordered (Supplemental Figs. S8, S9). Figure 5A shows the amino acid sequence of this region from four RsgI homologs. All four IDRs have similar compositional bias, enriched in charged and polar amino acids and depleted in aromatic and hydrophobic residues, but their frequency and arrangement differ. To investigate whether the *B. subtilis* IDR plays a role in regulating intramembrane proteolysis, we generated a deletion that lacked the last 157 amino acids (*rsgI*ΔID) and compared σ^I activity in wild type and the Δ*ponA* mutant. In *ponA*$^+$ cells, σ^I activity was similar whether or not the IDR was present (Fig. 5B). However, the *rsgI*ΔID mutant failed to activate σ^I in the absence of PBP1 (Δ*ponA*) (Fig. 5B). Analysis of GFP-RsgIΔID-His by immunoblot supports the idea that the IDR is required to sense envelope stress and trigger intramembrane proteolysis. As can be seen in Figure 5C and Supplemental Figure S12, the site-1-cleaved GFP-RsgIΔID-His products in both wild type and the Δ*ponA* mutant remained stable over 30 min. We note that the C-terminal GFP-RsgIΔID-His cleavage product could be resolved into two discrete bands due to its smaller size (Fig. 5C; Supplemental Fig. S12). The smaller of the two was stable over 30 min, while the larger one was lost. Analysis of these cleavage products and those from full-length RsgI suggests that the smaller product stably associates with its N-terminal partner, while the large one cannot (Supplemental Fig. S14). This provides an explanation for why cells harboring RsgIΔID retain basal σ^I activity (Fig. 5B) and are viable in a Δ*ponA* mutant (Fig. 5C), while cells lacking RasP have significantly lower σ^I activity (Fig. 1C) and are synthetic lethal with Δ*ponA* (Supplemental Fig. S4E).

Our analysis of the RsgIΔID suggests that the IDR on RsgI is important for sensing and responding to envelope stress. To investigate whether the amino acid composition of the IDR is important for sensing envelope stress, we generated chimeras between *B. subtilis* RsgIΔID and the IDRs from *Bacillus cereus*, *Bacillus pumilus*, and *Paenibacillus luteus* (Fig. 5A). In all three cases these domains restored inducible σ^I activity (Fig. 5B), suggesting that intrinsic disorder rather than a specific sequence is required

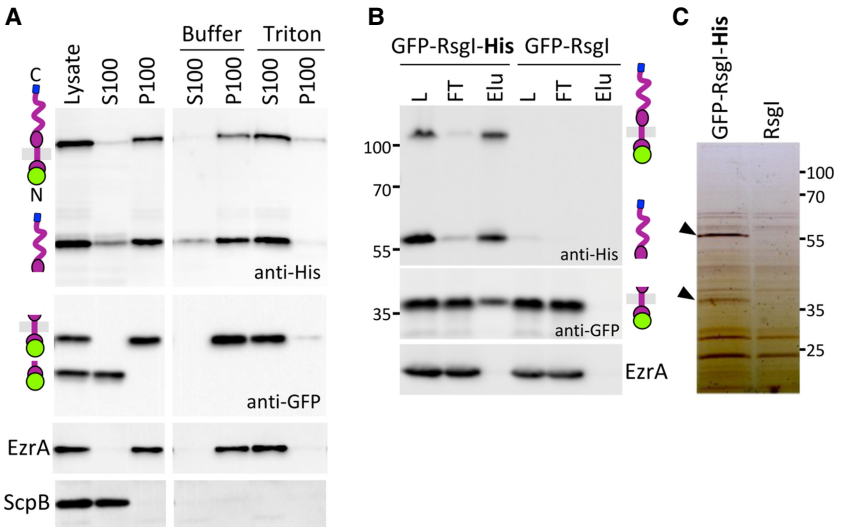

Figure 4. Site-1-cleaved RsgI products remain associated. (*A*) Representative immunoblots of GFP-RsgI-His fractionation. Protoplasts were generated from exponentially growing *B. subtilis* cells expressing GFP-RsgI-His. The protoplasts were washed in hypertonic buffer to remove proteins that were not membrane-associated and then lysed in hypotonic buffer, and the lysate was subjected to ultracentrifugation to separate soluble (S100) and membrane-associated (P100) proteins. The membrane fraction was dispersed in buffer or buffer containing Triton X-100 and subjected to a second round of ultracentrifugation to separate detergent-solubilized proteins (S100) from insoluble material (P100). Equivalent amounts of each fraction were separated by SDS-PAGE and analyzed by immunoblot. Full-length GFP-RsgI-His and both N-terminal and C-terminal site-1 cleavage products fractionated with the membrane. The N-terminal GFP-RsgI site-2 cleavage product was soluble. The membrane protein EzrA and cytoplasmic protein ScpB served as fractionation controls. (*B*) Immunoblots of Ni^{2+} affinity purifications from detergent-solubilized membrane fractions of *B. subtilis* cells expressing GFP-RsgI-His or GFP-RsgI. The load (L), flowthrough (FT), and elution (Elu) are shown. EzrA served as a negative control. Molecular weight markers are in kilodaltons. (*C*) Silver-stained gel of elutions from a similar purification from *B. subtilis* expressing GFP-RsgI-His or RsgI. N-terminal and C-terminal site-1 cleavage products identified by mass spectrometry are indicated (black carets). A silver-stained gel from a complementary coimmunoprecipitation experiment using anti-His antibody resin is shown in Supplemental Figure S10.

to respond to envelope stress. To further explore this possibility, we scrambled the order of the amino acids in the native *B. subtilis* IDR (Supplemental Fig. S15). We tested two scrambled IDRs, and both retained inducible σ^I activity (Fig. 5D). In contrast, replacing the IDR with the folded extracellular domain of the sporulation protein SpoIVFA (4FA) failed to support regulated σ^I activity (Fig. 5B). Importantly, analysis of the *B. cereus* and 4FA chimeras by immunoblot indicates that the impact on σ^I activity correlates with regulated proteolysis of RsgI (Fig. 5C; Supplemental Fig. S12). These data indicate that an intrinsically disordered region on RsgI is required to respond to envelope stress and are consistent with a model in which RsgI's IDR monitors the cell wall and, in the presence of defects or gaps in the meshwork, generates a pulling force that pulls the two site-1-cleaved products apart, triggering intramembrane proteolysis and σ^I activation (see the Discussion).

Class A PBPs have IDRs that can support RsgI signaling

In the course of our analysis of the IDR on RsgI homologs, we discovered that *B. subtilis* PBP1 and homologs in many Gram-positive bacteria contain similar intrinsically disordered regions at their extreme C termini (Fig. 6A; Supplemental Fig. S16). IDRs from a few of these homologs are shown in Figure 6A and Supplemental Figure S17. To investigate whether these regions can substitute for the IDR on RsgI, we generated chimeras and tested them for the regulation of σ^I activity. Although the IDR from *B. subtilis* PBP1 did not restore activity when appended to RsgIΔID, three distinct IDRs from PBP1 homologs from different *B. cereus* strains all restored RsgIΔID's ability to respond to the absence of *B. subtilis* PBP1 (Fig. 5B). These data suggest that many but not all aPBP IDRs are functional in responding to envelope defects and raised the possibility that class A PBPs could use their IDRs to direct cell wall synthesis to sites that require repair.

The IDR on PBP1 promotes efficient cell wall synthesis

To investigate whether PBP1's IDR is important for its function, we deleted the 121-amino-acid C-terminal IDR, leaving the adjacent fibronectin type III (FN3) domain intact (Fig. 6A). We fused the full-length gene and the deletion mutant to an IPTG-regulated promoter and compared growth in an aPBP-deficient strain. In the presence of 100 µM IPTG, both PBP1 variants restored normal colony size to the aPBP mutant (Supplemental Fig. S18A). However, when their levels were reduced using 15 µM IPTG, only full-length PBP1 restored normal colony size and cell morphology, while cells expressing the PBP1ΔID grew more slowly (Supplemental Fig. S18A), had morphological defects (Supplemental Fig. S19), and induced σ^I activity (Supplemental Fig. S18B). Importantly, appending IDRs from PBP1 or RsgI homologs onto PBP1ΔID restored wild-type growth and morphology and suppressed σ^I induction (Supplemental Figs. S18, S19). In contrast, fusing the folded extracellular domain of SpoIVFA (4FA) onto PBP1ΔID phenocopied the ΔID mutant (Supplemental Figs. S18, S19).

To more rigorously test whether disparate IDRs are functional when appended onto PBP1ΔID, we sought a sensitized background that would enhance the growth and morphology defects of the ΔID mutant. The GpsB protein is thought to function as a cytoplasmic scaffold for

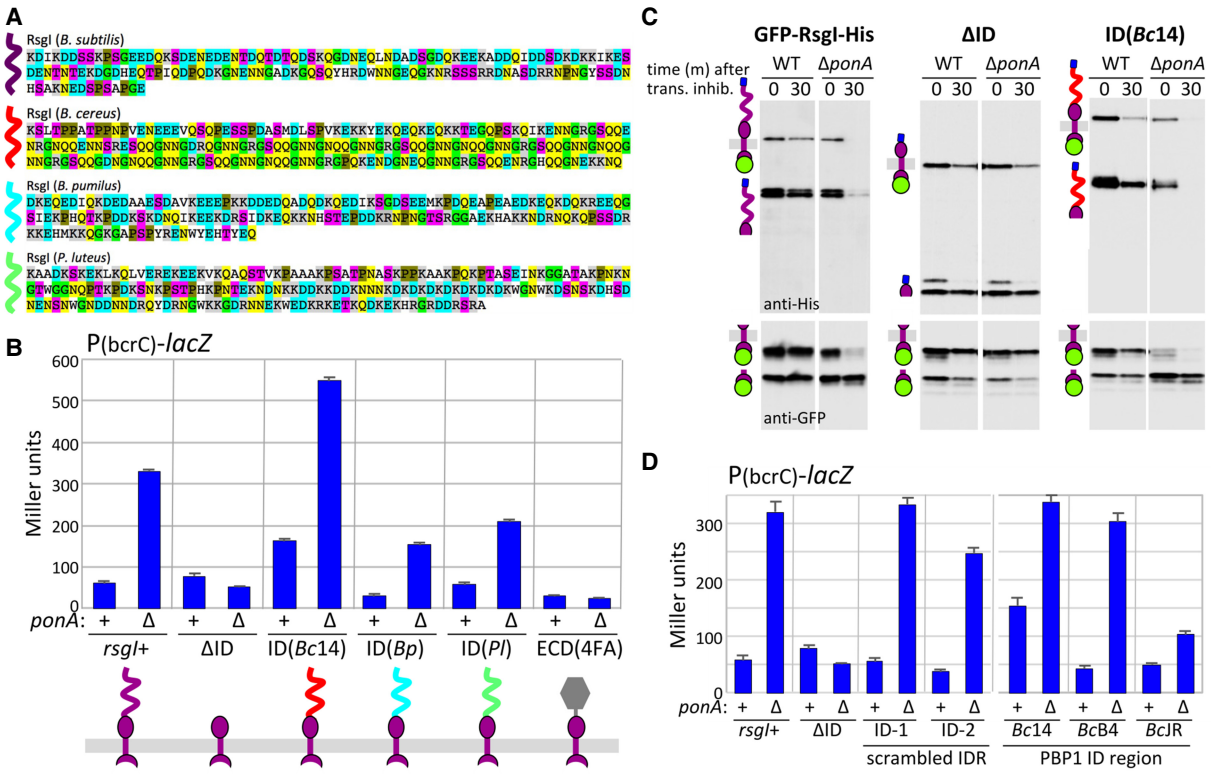

Figure 5. An intrinsically disordered region on RsgI is required to respond to loss of the PG synthase PBP1. (*A*) Examples of the intrinsically disordered (ID) regions on RsgI homologs from *B. subtilis*, *Bacillus cereus*, *Bacillus pumilus*, and *Paenibacillus luteus.* Residues with similar properties are highlighted with the same color. An alignment of 26 RsgI homologs is shown in Supplemental Figure S8 and Supplemental Table S4. (*B*) Bar graph showing β-galactosidase activity from the σ^I-responsive reporter P(bcrC)-*lacZ* in the presence (+) or absence (Δ) of *ponA*. All strains lack the native *rsgI* gene and harbor the indicated *rsgI* variant at an ectopic locus. The *rsgI* variant lacking its ID region (ΔID) and the one with the ID region replaced with the extracellular domain (ECD) of the *B. subtilis* sporulation protein SpoIVFA (4FA) do not respond to the absence of PBP1. (*C*) Stability assays of the GFP-RsgI-His cleavage products. Immunoblot analysis of GFP-RsgI-His, GFP-RsgIΔID-His (ΔID), and GFP-RsgIΔID-ID(Bc14)-His [ID(Bc14)] in wild-type and Δ*ponA* backgrounds. Strains were grown in LB medium supplemented with 10 mM (WT) or 20 mM [ΔID and ID(Bc14)] xylose to midexponential phase. Cultures were then treated with spectinomycin and chloramphenicol to inhibit protein synthesis. Samples were collected before and 30 min after addition of the translation inhibitors, and GFP-RsgI-His was assessed by immunoblot using anti-GFP and anti-His antibodies. For a full time course of these and other RsgI chimeras, see Supplemental Figure S11. (*D*) Bar graph showing β-galactosidase activity from a σ^I-responsive reporter in the indicated strains lacking the native *rsgI* gene. The amino acids in the *B. subtilis* ID region were scrambled, and separately the ID regions from PBP1 homologs from three *B. cereus* strains were fused to *rsgI*ΔID. Activity was assayed in exponentially growing cultures in LB. Error bars represent standard deviation from three biological replicates. The P(bcrC)-*lacZ* reporter was inserted at an origin-distal chromosomal locus in the strains used in this figure, accounting for the reduced response compared with those in Figure 1 (see Supplemental Fig. S13).

PBP1 and other membrane proteins involved in PG synthesis (Cleverley et al. 2019). Accordingly, we compared PBP1 and PBP1ΔID in a Δ*gpsB* background. As can be seen in Figure 6B, the PBP1ΔID mutant was severely growth-impaired when expressed using 50 µM IPTG. The growth defect was even more pronounced using 25 µM IPTG but was also apparent at concentrations as high as 250 µM IPTG (Supplemental Fig. S20). As can be seen in Figure 6B, the PBP1ΔID mutant was severely growth-impaired. The growth defect was pronounced using 25 µM IPTG but was readily apparent at 50 and 250 µM IPTG (Supplemental Fig. S20). Importantly, in this sensitized background, the PBP1ΔID mutant cells were thinner, twisted, and more prone to lysis compared with full-length PBP1 (Fig. 6D; Supplemental Fig. S21). PBP1 chimeras harboring IDRs from PBP1 and RsgI homologs as well as two scrambled versions of the native PBP1 IDR largely restored normal growth and morphology, while a chimera that contained the folded 4FA ECD did not (Fig. 6A,D; Supplemental Figs. S20–S22). In all cases, these variants were produced at levels similar to full-length PBP1 (Fig. 6B; Supplemental Fig. S20A). Finally, we show in Figure 6E that purified PBP1 lacking its IDR retained wild-type glycosyltransferase activity in vitro, suggesting that the requirement for the IDR on PBP1 is not related to its enzymatic activity. Collectively, these data indicate that an intrinsically disordered region on PBP1 is required for the full function of the PG synthase and are consistent with a model in which the IDR helps localize PBP1 to sites in the PG meshwork that require fortification or repair.

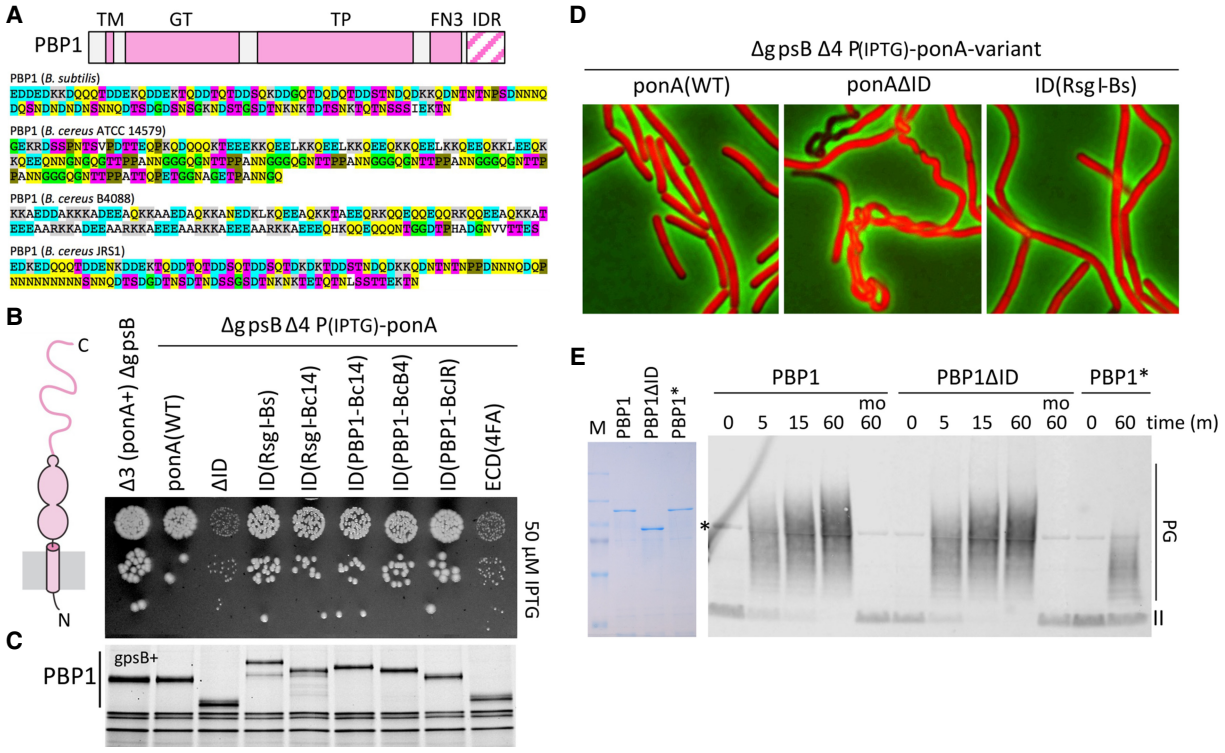

Figure 6. The IDR on PBP1 is important for function. (*A*) Schematic diagram of *B. subtilis* PBP1 showing the transmembrane (TM) segment, the glycosyltransferase (GT) and transpeptidase (TP) domains, the fibronectin 3-like (FN3) domain, and the intrinsically disordered region (IDR). The IDRs from *B. subtilis* PBP1 and three *B. cereus* strains are shown *below*. Residues with similar properties are highlighted with the same color. (*B*) Schematic of PBP1 and spot dilutions on LB agar plates supplemented with 50 µM IPTG. The first strain lacks *gpsB* and three of the four aPBP genes (Δ3) and is *ponA*$^+$. All other strains lack *gpsB* and the four native aPBP genes (Δ4). The indicated variants of *ponA* are expressed under IPTG control. (*C*) Bocillin gel of the *gpsB*$^+$ versions of the strains in *B*. (*D*) Representative fluorescence and phase-contrast images of cells expressing wild-type *ponA* or the variant with its IDR (ΔID) lacking or replaced with the IDR from *B. subtilis* RsgI. All three strains lack *gpsB* and the four native aPBP genes (Δ4) and expressed cytoplasmic GFP. Cells were grown in LB medium with 100 µM IPTG and subcultured for three to four generations in LB with 25 µM IPTG. (*E*) PBP1ΔID has glycosyltransferase activity similar to that of the full-length PBP1 protein. Coomassie-stained gel of the purified proteins used in the GT assay. PBP1* has an E115A substitution in the predicted GT catalytic residue. Representative Western blot of glycan strand polymerization assay using purified proteins and lipid II. Time points (in minutes) are indicated *above* the blot. The reaction products and remaining substrate were labeled with biotinylated D-lysine using *S. aureus* PBP4, resolved by SDS-PAGE, and detected by IRDye 800CW streptavidin. A 60-min time point in the presence of the GT inhibitor moenomycin (mo) is shown. Free lipid II (II) and glycan strands (PG) are indicated. Some PBP4 became biotinylated in the labeling reaction and was detected (asterisk) by IRDye 800CW streptavidin.

Discussion

Previous work by Helmann and coworkers (Patel et al. 2020) established that cells lacking PBP1 require σ^I for viability and that σ^I activity increases in cells that lack PBP1. Here, we have confirmed and extended these findings and shown that σ^I activity inversely correlates with the level of the PG synthase. These data suggest that the RsgI–σ^I pathway responds in a graded manner to reduced PG synthesis and therefore functions in cell wall homeostasis. Our analysis has further revealed that intrinsically disordered regions lie at the heart of cell wall maintenance. We have shown that the IDR on RsgI is required to activate σ^I in cells lacking PBP1, while the IDR on PBP1 is necessary for the full function of the PG synthase. Since IDRs from RsgI homologs can function on *B. subtilis* PBP1 and since most PBP1 IDRs can function on *B. subtilis* RsgI, our data further suggest that these regions act similarly on both proteins. Importantly, both RsgI and PBP1 are functional when the order of the amino acids in their native IDRs is scrambled, indicating that disorder is central to their activity. It is currently unknown how these unstructured regions function or what they do in the Gram-positive periplasm, but the simplest interpretation of our data, given that these IDRs are appended to a factor that responds to cell wall defects and an enzyme that synthesizes peptidoglycan, is that they enter gaps in the PG meshwork (Fig. 7). In the case of RsgI, interaction with the PG that lines the gap could generate force to activate σ^I (discussed below), and in the case of PBP1 it would transiently localize the synthase to this site to repair it, akin to the Lpo factors in Gram-negative bacteria (Vigouroux et al. 2020). Recent high-resolution atomic force microscopy (AFM) studies of the *B. subtilis* cell wall identified gaps or holes in the membrane-proximal layers of the meshwork that range in size from 5 to 8 nm in diameter (Pasquina-Lemonche et al.

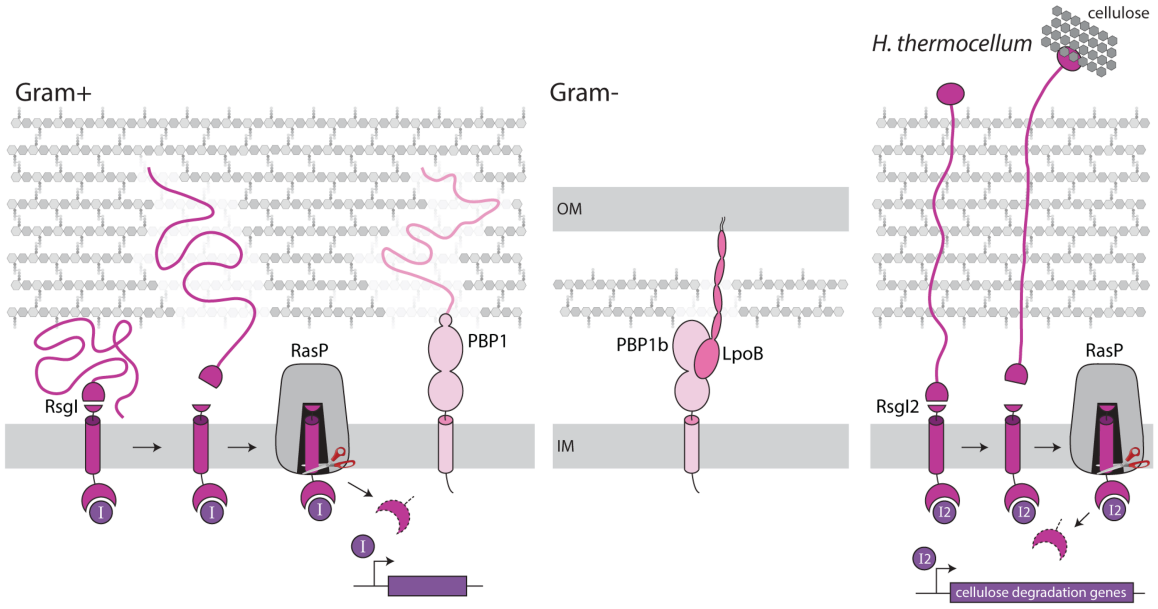

Figure 7. Intrinsically disordered regions sense defects in the Gram-positive cell wall. Model for intrinsically disordered regions on RsgI and PBP1. σ^I (I) is held inactive at the membrane by RsgI. RsgI is constitutively cleaved by an unknown site-1 protease, but the two products remain stably associated. When the IDR on RsgI encounters a gap in the cell wall meshwork, it enters this region, resulting in dissociation of the two cleaved products, which enables intramembrane proteolysis by the site-2 protease RasP. Intramembrane proteolysis leads to release of σ^I and activation of genes that help repair the defect. The IDR on PBP1 transiently restrains the PG synthase at these same gaps in the meshwork, facilitating their repair. The function of the IDR on PBP1 is analogous to the transenvelope interaction between Lpo factors and their cognate aPBPs in Gram-negative bacteria. The RsgI2 paralog in *C. thermocellum* has a carbohydrate-binding module (CBM) appended to the end of its intrinsically disordered region. This domain binds extracellular cellulose and activates SigI2 that controls genes involved in cellulose degradation. We hypothesize that SigI2 activation is mediated by an analogous mechanotransduction pathway in which cellulose binding to the CBM pulls the cleaved RsgI2 apart and activates intramembrane proteolysis. In this model, the IDR on RsgI2, which has a distinct amino acid composition, threads through the wall rather than filling gaps.

2020). Some of these gaps appear to extend through multiple layers of the sacculus and, if unattended, could lead to lysis. The work presented here suggests that RsgI and PBP1 and their associated IDRs represent complementary pathways that sense and respond to these defects.

It is noteworthy that cells harboring PBP1 lacking its IDR (PBP1ΔID) only displayed growth and morphological defects when expressed at low levels or in a sensitized background lacking GpsB. These data indicate that, unlike Gram-negative Lpo factors (Paradis-Bleau et al. 2010; Typas et al. 2010), the IDR on PBP1 is not essential for PBP1 activity. However, despite the normal growth and morphology of cells expressing wild-type levels of PBP1ΔID, σ^I-dependent gene expression was induced (Supplemental Fig. S23). These findings suggest that IDR-less PG synthases produce sufficient quantities of cell wall material to maintain growth and morphology but lack the ability to identify gaps in the meshwork and therefore inefficiently fill them, leading to their detection by RsgI and, in turn, activation of σ^I.

σ^I controls the expression of a small set of factors involved in cell wall biogenesis that includes the PG hydrolase LytE, the MreB paralog MreBH, and the undecaprenyl-pyrophosphate (UndPP) phosphatase BcrC that recycles the lipid carrier UndP. How these factors function to repair defects in the meshwork is currently unknown. However, work in *E. coli* indicates that overexpression of PG endopeptidases required for cell wall expansion stimulates PG synthesis (Lai et al. 2017), and the increase in LytE expression under σ^I control could function similarly here. An alternative but not mutually exclusive model is that LytE could enlarge the gaps in the meshwork, enabling repair by Rod complexes organized by MreBH. Future experiments will be focused on establishing how the factors under σ^I control promote PG synthesis and repair.

Mechanotransduction as a possible mechanism of σ^I control.

Previous genetic analyses had implicated the S2P/RseP family member RasP in the control of σ^I activity (Liu et al. 2017; Patel et al. 2020). Here, we demonstrated that the anti-σ^I factor RsgI is indeed subject to regulated intramembrane proteolysis. However, unlike canonical RIP signaling pathways, our data indicate that site-1 cleavage of RsgI is constitutive, but the cleaved products remain stably associated, preventing intramembrane proteolysis by the site-2 protease. Instead, the regulated step in this signaling pathway is the dissociation of the cleaved ectodomain, which triggers intramembrane proteolysis and σ^I activation.

This RsgI–σ^I signaling pathway shares strikingly similar features with mechanotransduction pathways involved in

metazoan development. The Notch transcription factor plays a central role in the communication between adjacent cells to modulate cell fate decisions and is controlled by an unrelated intramembrane-cleaving protease, γ secretase (Kopan and Ilagan 2009; Sprinzak and Blacklow 2021). Surface-anchored ligands of the Delta–Serrate–lag-2 (DSL) family on a signal-sending cell interact with membrane-anchored Notch receptors on a signal-receiving cell. Internalization of the Notch–ligand complex via receptor-mediated endocytosis in the signal-sending cell is thought to generate a pulling force that causes a conformational change in the juxtamembrane domain of Notch on the signal-receiving cell (Nichols et al. 2007; Musse et al. 2012; Gordon et al. 2015). The conformational change exposes a sterically occluded protease site, and cleavage at this position by a site-1 protease releases the ectodomain and triggers intramembrane proteolysis by γ secretase (Kopan and Ilagan 2009; Sprinzak and Blacklow 2021). The intracellular domain then enters the nucleus and controls developmental gene expression. Similarly, adhesion G protein-coupled receptors (aGPCRs) control tissue specification during development by transducing information received from adjacent cell surface proteins or components of the extracellular matrix (ECM) (Bjarnadóttir et al. 2004; Langenhan et al. 2013). aGPCRs contain a juxtamembrane autoproteolysis domain that cleaves the nascent receptor into two fragments that remain stably associated, concealing a peptide agonist. It is thought that the interaction between the extracellular domain and the ECM or surface ligands on neighboring cells generates a pulling force that dissociates the ectodomain, exposing the tethered agonists that trigger G protein activation (Liebscher et al. 2014; Stoveken et al. 2015). Thus, in both cases, a pulling force triggers information transduction across the lipid bilayer.

The force that dissociates the site-1-cleaved ectodomain of RsgI is currently unknown. However, we have shown that dissociation requires the presence of an extracytoplasmic IDR. Importantly, even IDRs in which the order of the amino acids was scrambled retained their signaling function. This finding argues that the IDR does not function by templated folding upon recognition of some feature of the cell envelope. Instead, we hypothesize that nonspecific multivalent interactions between the charged and polar residues in the IDR and the PG that lines the gap in the meshwork generate force. Defining the length requirement and amino acid composition for a functional IDR on RsgI in vivo and determining the force necessary to dissociate the ectodomain in vitro are the first steps toward establishing whether σ^I activation is controlled by mechanotransduction.

Interestingly, RsgI homologs in the bacterium *Clostridium thermocellum* may have evolved a distinct mechanism of force generation. This bacterium assembles large multienzyme complexes called cellulosomes on its cell surface that efficiently convert plant cell wall polysaccharides like cellulose and hemicellulose into soluble sugars (Artzi et al. 2017). *C. thermocellum* contains eight *sigI–rsgI* loci (Kahel-Raifer et al. 2010). Several of the σ^I paralogs encoded in these bicistronic operons control cellulosome-associated enzymes involved in plant cell wall degradation and are induced in the presence of cellulose and related polysaccharides in the medium (Kahel-Raifer et al. 2010; Nataf et al. 2010; Muñoz-Gutiérrez et al. 2016; Ortiz de Ora et al. 2018). The cognate RsgI paralogs have conserved juxtamembrane domains that resemble the one from *B. subtilis* and are followed by an IDR. Importantly, several of these paralogs have carbohydrate-binding modules (CBMs) that bind plant polysaccharides appended to the C termini of their IDRs (Fig. 7; Kahel-Raifer et al. 2010; Nataf et al. 2010; Yaniv et al. 2013). Since cellulose and related carbohydrates are too large to enter the PG meshwork, it has been proposed that the IDRs span the *C. thermocellum* envelope, displaying the CBMs on the cell surface. How biomass sensing is transduced across the lipid bilayer has remained a mystery. Based on the work presented here, we hypothesize that cellulose bound to the CBM generates a shear force that pulls the site-1-cleaved RsgI products apart, triggering site-2 proteolysis and activation of the cognate σ^I. Although it is currently unknown whether *C. thermocellum* RsgI paralogs are regulated by intramembrane proteolysis, this mechanotransduction model provides a novel mechanism by which Gram-positive bacteria could sense and respond to macromolecules in their environment. It is noteworthy that the IDRs on the *C. thermocellum* RsgI paralogs that possess CBMs have many fewer polar and charged residues compared with the IDRs characterized here. This difference could ensure that the *C. thermocellum* IDRs interact more weakly with the PG meshwork that they span, enabling them to function as neutral linkers that transduce the force applied to the polysaccharide–CBM complex to the juxtamembrane domain. Analysis of chimeras between these RsgI paralogs and *B. subtilis* RsgI in the future will help test this model and have the potential to establish whether these biomass-sensing signaling pathways also involve mechanotransduction.

Materials and methods

General methods

All *B. subtilis* strains were derived from the prototrophic strain PY79 (Youngman et al. 1983). Unless otherwise indicated, cells were grown in LB or defined rich (casein hydrolysate [CH]) medium (Harwood and Cutting 1990) at 37°C. Insertion–deletion mutations were generated by isothermal assembly (Gibson 2011) of PCR products followed by direct transformation into *B. subtilis*. Tables of strains, plasmids, and oligonucleotide primers are available as Supplemental Tables S1–S3, and a description of strain and plasmid construction is in the Supplemental Material.

β-Galactosidase assays

B. subtilis strains were grown in LB medium at 37°C to an OD_{600} of ~0.7. The optical density was recorded, and 1 mL of culture was harvested and assayed for β-galactosidase activity as previously described (Rudner et al. 1999). Briefly, cell pellets were resuspended in 1 mL of Z buffer (40 mM NaH_2PO_4, 60 mM Na_2HPO_4, 1 mM $MgSO_4$, 10 mM KCl, 50 mM β-mercaptoethanol). Two-hundred-fifty microliters of this suspension was added to 750 µL of Z buffer

supplemented with 0.25 mg/mL lysozyme, and the samples were incubated for 15 min at 37°C. The colorimetric reaction was initiated by addition of 200 µL of 4 mg/mL 2-nitrophenyl-β-D-galactopyranoside (ONPG) in Z buffer and stopped with 500 µL of 1 M Na_2CO_3. The reaction time and the absorbance at 420 nm and OD_{550} of the reactions were recorded, and the β-galactosidase-specific activity in Miller units was calculated according to the formula $[A_{420} - 1.75 \times (OD_{550})]/[\text{time (minutes)} \times OD_{600}] \times \text{dilution factor} \times 1000$ (Miller 1972).

Immunoblot analysis

Immunoblot analysis was performed as described previously (Wang et al. 2015). Briefly, 1 mL of culture was collected and resuspended in lysis buffer (20 mM Tris at pH 7.0, 10 mM $MgCl_2$, 1 mM EDTA, 1 mg/mL lysozyme, 10 µg/mL DNase I, 100 µg/mL RNase A, 1 mM PMSF, 1 µg/mL leupeptin, 1 µg/mL pepstatin) to a final OD_{600} of 10 for equivalent loading. The cells were incubated for 10 min at 37°C, followed by addition of an equal volume of sodium dodecyl sulfate (SDS) sample buffer (0.25 M Tris at pH 6.8, 4% SDS, 20% glycerol, 10 mM EDTA) containing 10% 2-mercaptoethanol. Samples were heated for 15 min at 65°C prior to loading. Proteins were separated by SDS-PAGE on 12.5% polyacrylamide gels, electroblotted onto immobilon-P membranes (Millipore), and blocked in 5% nonfat milk in phosphate-buffered saline (PBS) with 0.5% Tween-20. The blocked membranes were probed with anti-LytE (1:10,000) (Dobihal et al. 2019), anti-SigA (1:10,000) (Fujita and Sadaie 1998), anti-His (1:4000; Sigma), and anti-GFP (1:10,000) (Rudner and Losick 2002) antibodies diluted into 3% BSA in PBS with 0.05% Tween-20. Primary antibodies were detected using horseradish peroxidase-conjugated goat anti-rabbit or antimouse IgG (Bio-Rad) and the Super Signal chemiluminescence reagent as described by the manufacturer (Pierce). Signal was detected using a Bio-Techne FluorChem R system.

In vivo protein turnover assay

B. subtilis strains were grown in LB medium at 37°C to an OD_{600} of 0.5. Protein translation was inhibited by the addition of both spectinomycin (200 µg/mL final concentration) and chloramphenicol (10 µg/mL final concentration). One-milliliter samples were collected immediately prior to antibiotic treatment and at the indicated times after. Cells were pelleted by centrifugation for 5 min and immediately flash-frozen in liquid nitrogen. The cell pellets were thawed on ice, lysed, and analyzed by immunoblot as described above.

Bocillin labeling

B. subtilis strains were grown in LB medium supplemented with the indicated concentrations of IPTG at 37°C to an OD_{600} of ~0.7. Ten milliliters of cells was pelleted, washed with PBS, resuspended with 100 µL of PBS containing 15 µM bocillin (Invitrogen), and incubated for 15 min at 22°C. Cells were washed three times with PBS, resuspended in 0.5 mL of PBS containing 1 mg/mL lysozyme, and incubated for 30 min at 37°C. The cells were lysed by sonication, followed by a low-speed spin at 3000*g* for 5 min to remove unbroken cells. The lysate was subjected to ultracentrifugation at 100,000*g* for 45 min at 4°C. The membrane pellet was resuspended with 50 µL of sample buffer, and total protein was determined using the NI protein assay (G-Biosciences). Twenty micrograms of total protein was incubated for 20 min at 65°C and resolved by SDS-PAGE on 10% polyacrylamide gels. Bocillin-labeled proteins were visualized using a Typhoon 9500 fluorescence imager (GE Healthcare) with excitation at 488 nm and emission at 530 nm.

Fluorescence microscopy

Fluorescence microscopy was performed on a Nikon Ti microscope equipped with a plan apo 100×/1.4 NA phase-contrast oil objective and a CoolSnapHQ^2 camera. Cells were immobilized using 1.5% agarose pads containing LB medium. Envelope integrity was monitored with 5 µM propidium iodide (PI; Molecular Probes). Exposure times were 200, 300, and 800 msec for phase, PI, and mCherry, respectively. Images were cropped and adjusted using MetaMorph software (Molecular Devices).

Transposon insertion sequencing

Transposon insertion sequencing (Tn-seq) was performed as described previously (van Opijnen et al. 2009; Johnson and Grossman 2014; Meeske et al. 2015). Libraries of >100,000 independent transposants were separately generated in wild type or Δ*cwlO*, Δ*sigI*, or Δ*ponA* mutants. Genomic DNA was extracted from each library and digested with MmeI, followed by adapter ligation. Transposon–chromosome junctions were amplified by PCR (17 amplification cycles). PCR products were pooled, gel-purified, and sequenced on the Illumina HiSeq platform using TruSeq reagents (Tufts University Core Facility Genomics Facility). Reads were mapped to the *B. subtilis* 168 genome (NCBI NC_000964.3) and tallied at each TA site, and genes in which reads were statistically underrepresented were identified using the Mann–Whitney *U*-test and by visual inspection using Sanger Artemis genome browser and annotation tool (Carver et al. 2012).

Rsgi fractionation

Twenty-five milliliters of exponentially growing cells of strain BYB1156 (PxylA-GFP-RsgI-His) was collected, washed, and resuspended in 5 mL of 1× SMM buffer (0.5 M sucrose, 20 mM $MgCl_2$, 20 mM maleic acid at pH 6.5) (Harwood and Cutting 1990) supplemented with 2 mg/mL lysozyme. Cells were gently agitated for 30 min at room temperature. When >95% of the cells had converted to protoplasts as assayed by microscopic observation, they were collected by centrifugation at 5000 rpm, washed twice in 1× SMM, and lysed with 1 mL of hypotonic buffer (buffer H: 20 mM HEPES at pH 8, 200 mM NaCl, 1 mM dithiothreitol) with protease inhibitors (1 mM phenylmethylsulfonyl fluoride and EDTA-free protease inhibitor cocktail complete [Roche]). $MgCl_2$ and $CaCl_2$ were added to 1 mM, and lysates were treated with 10 µg/mL DNase I (Sigma-Aldrich) and 20 µg/mL RNase A (USB) for 1 h on ice. The membrane fraction was separated by ultracentrifugation at 200,000*g* for 1 h at 4°C. The supernatant was carefully removed, and the membrane pellet was dispersed in 100 µL of buffer H. The dispersed membranes were split into two aliquots, incubated with buffer H with or without 1% Triton X-100 for 1 h at 4°C, and separated by ultracentrifugation at 200,000*g* for 1 h at 4°C. The supernatant and pellet fractions were then analyzed by immunoblot as described above.

Rsgi purification and mass spectrometry identification

Strains BDR11 (WT), BYB1156 (PxylA-GFP-RsgI-His), and BYB1123 (PxylA-GFP-RsgI) were precultured in LB to an OD_{600} of 0.4 and used to inoculate 500 mL of LB supplemented with xylose (30 mM final concentration) at an OD_{600} of 0.01. Strains were grown at 37°C with aeration until an OD_{600} of 0.4. Cells were collected by centrifugation at 5000 rpm, washed twice in 50 mL of 1×

SMM, and resuspended in 20 mL of 1× SMM with lysozyme (0.5 mg/mL final concentration). The suspension was gently agitated for ~30 min at room temperature until >95% of the cells had formed protoplasts as monitored by phase-contrast microscopy. The protoplasts were divided into two 10-mL aliquots, pelleted by centrifugation at 5000 rpm for 5 min, and flash-frozen in N_2(l). Lysates were generated from individual aliquots (equivalent to 250 mL of culture) by the addition of 3 mL of hypotonic buffer (buffer H: 20 mM HEPES at pH 7.6, 200 mM NaCl, 1 mM dithiothreitol) supplemented with 1× complete protease inhibitor (Roche) and 125 U of benzonase (Sigma). Lysates were incubated for 1 h on ice, followed by centrifugation at 5000 rpm for 10 min at 4°C to pellet cell debris. The supernatant was subjected to ultracentrifugation at 200,000*g* for 1 h at 4°C. The membrane pellet was dispersed in 200 µL of buffer H with 10% glycerol and flash-frozen in two aliquots. Detergent solubilization of membrane proteins was performed on individual aliquots by mixing the thawed membranes with 500 µL of solubilization buffer (buffer S: buffer H containing 20% glycerol, 1% Triton X-100). The mixture was rotated for 1 h at 4°C and then subjected to ultracentrifugation at 100,000*g* for 1 h at 4°C. The supernatant containing detergent-solubilized proteins was mixed with 25 µL of Ni^{2+}-NTA resin (Qiagen), equilibrated with buffer S, and rotated for 2 h at 4°C. The resin was pelleted by centrifugation at 3000 rpm for 2 min at 4°C, washed three times with 500 µL of buffer S containing 30 mM imidazole, and eluted with 50 µL of buffer S containing 300 mM imidazole. The eluted proteins were resolved by SDS-PAGE on a 12.5% polyacrylamide gel and visualized by silver staining (Bio-Rad) or immunoblot as described above. Individual silver-stained bands were excised and treated with trypsin or chymotrypsin, and the eluted peptides were identified by mass spectrometry (Taplin Mass Spectrometry Facility, Harvard Medical School). The MS identified 14 unique peptides in the His-tagged C-terminal domain of RsgI and 16 unique peptides in the GFP-tagged N-terminal domain, nine of which were unique to GFP.

Coimmunoprecipitation and protein identification using anti-His antibody resin (Genscript) were performed identically except imidazole was excluded from all buffers and immunoprecipitated proteins were eluted with 50 µL of 2× SDS-sample buffer without BME. Ten percent BME was added prior to SDS-PAGE.

Purification of PBP1 and variants

E. coli strain BL21 DE3 Δ*tonA* was transformed with plasmid pYB259 (His-SUMO-ponA), pCH037 [His-SUMO-ponA(E115A)], or pYB260 (His-SUMO-ponAΔID), and fresh transformants were precultured in Terrific broth (TB) supplemented with 100 µg/mL ampicillin. Cultures were rolled at 37°C until an OD_{600} of 0.4 and then were used to inoculate 1 L of TB supplemented with 100 µg/mL ampicillin at an OD_{600} of 0.01. The cultures were grown at 37°C with shaking until an OD_{600} of 0.2, at which time they were moved to a 20°C shaker. When the OD_{600} reached 0.4, IPTG was added to 0.5 mM final concentration, and the cultures were grown overnight at 20°C. Cells were harvested by centrifugation at 5000 rpm for 15 min, resuspended in 50 mL of buffer A (50 mM HEPES at pH 7.5, 500 mM NaCl, 10% glycerol), and frozen at −80°C.

The pellet from each strain was thawed and lysed by two passes through a cell disruptor at 25,000 PSI at 4°C (Constant System). Benzonase (125 U; Sigma) and 1× complete protease inhibitor (Roche) were added to each lysate and incubated for 15 min on ice. The lysates were subjected to ultracentrifugation at 40,000 rpm for 1 h at 4°C. The membrane pellets were dounce-homogenized in 30 mL of buffer B (20 mM HEPES at pH 7.5, 500 mM NaCl, 10% glycerol, 25 mM imidazole). Three milliliters of 10% (w/v) Triton X-100 was layered on top of dispersed membranes and rapidly mixed by inverting. The detergent/membrane mixture was then rolled for 1 h at 4°C, followed by ultracentrifugation at 40,000 rpm for 1 h at 4°C. The supernatant (S100) was applied to 1 mL of Ni^{2+}-NTA resin and then washed with 50 column volumes of buffer B + 0.1% Triton X-100. The protein was eluted with buffer B containing 350 mM imidazole and 0.1% Triton X-100. The peak fractions were pooled, treated with 6.25 µg of His-Ulp1 protease, and dialyzed overnight at 4°C in 2 L of buffer D (20 mM HEPES at pH 7.5, 500 mM NaCl, 0.1% Triton X-100, 10% glycerol, 5 mM BME). The dialyzed elutions were mixed with 1 mL of Ni^{2+}-NTA resin equilibrated with buffer D. The mixture was loaded onto a Bio-Rad column, and the flowthrough containing purified PBP1 variants was collected after three passes over the column. The flowthrough was concentrated using an Amicon centrifugal filter unit (MWCO 10 kDa), and the protein was analyzed for purity and concentration by SDS-PAGE using 10% polyacrylamide gels stained with Instant Blue (Abcam).

Glycosyltransferase activity assay

Glycosyltransferase (GT) activity assays were performed using a protocol adapted from Qiao et al. (2014). Reactions were performed in a 10-µL volume with 20 mM HEPES (pH 7.5), 20 mM MnCl2, 0.1% (w/v) Triton X-100, and 10 µM lipid II in DMSO (2% final concentration) purified from *E. faecalis* (Qiao et al. 2017). Moenomycin A (50 µM final concentration; gift from Suzanne Walker) was added where indicated. Reactions were initiated by the addition of 2 µL of recombinant PBP1, PBP1ΔID, or PBP1(E115A) at 1.25 µM final concentration and incubated for the indicated times at 25°C. Reactions were stopped by heat denaturation for 5 min at 95°C. Following inactivation, *S. aureus* PBP4 (5 µM final concentration) (Welsh et al. 2017) and biotinylated D-lysine (10 µM final concentration; Sigma) were added, and the samples were incubated for 1 h at 25°C. Reactions were quenched by the addition of 15 µL of 2× Laemmli SDS sample buffer containing 10% β-mercaptoethanol, and half the reaction was resolved by SDS-PAGE on a 4%–20% acrylamide gel for 80 min at 35 mA. The samples were transferred to a PVDF membrane and washed with PBS. The membrane was incubated in 0.4% paraformaldehyde for 1 h, washed with PBS, and then blocked for 1 h in SuperBlock (Thermo). The membrane was then incubated in SuperBlock with IRDye 800CW streptavidin (diluted 1:5000) for 1 h at room temperature. Membranes were washed three times in TBS/Tween20 and once in PBS and imaged using an Odyssey CLx system (LI-COR Biosciences).

Competing interest statement

The authors declare no competing interests.

Acknowledgments

We thank all members of the Bernhardt-Rudner supergroup past and present for helpful advice, discussions, and encouragement; the Harvard Medical School Microscopy Resources on the North Quad (MicRoN) Core for advice on microscopy and analysis; Genevieve Dobihal and Alex Meeske for sharing Tn-seq data; Ian Roney for building strains; Xindan Wang for insight about marker frequency analysis; and Marios Sardis, Lindsey Marmont, Caroline Midonet, Tom Bernhardt, Suzanne Walker, and Andrew Kruse for sharing reagents and expertise. Support for this work comes from the National Institutes of Health grants GM086466 and GM127399 (to D.Z.R.). Y.R.B. was funded in part by an

EMBO Long-Term Fellowship. A.P.B. was funded by the National Science Foundation (DGE1745303). L.A. is a Simons Foundation fellow of the Life Sciences Research Foundation.

Author contributions: Y.R.B., C.H., A.P.B., L.A., and D.Z.R. designed the research. Y.R.B., C.H., A.P.B., and L.A. performed the research. Y.R.B., C.H., A.P.B., L.A., and D.Z.R. analyzed the data and wrote the paper.

References

Akiyama K, Mizuno S, Hizukuri Y, Mori H, Nogi T, Akiyama Y. 2015. Roles of the membrane-reentrant β-hairpin-like loop of RseP protease in selective substrate cleavage. *Elife* **4:** e08928. doi:10.7554/eLife.08928

Alba BM, Leeds JA, Onufryk C, Lu CZ, Gross CA. 2002. Degs and YaeL participate sequentially in the cleavage of RseA to activate the σ^E-dependent extracytoplasmic stress response. *Genes Dev* **16:** 2156–2168. doi:10.1101/gad.1008902

Artzi L, Bayer EA, Moraïs S. 2017. Cellulosomes: bacterial nanomachines for dismantling plant polysaccharides. *Nat Rev Microbiol* **15:** 83–95. doi:10.1038/nrmicro.2016.164

Asai K, Ootsuji T, Obata K, Matsumoto T, Fujita Y, Sadaie Y. 2007. Regulatory role of RsgI in sigI expression in *Bacillus subtilis*. *Microbiology* **153:** 92–101. doi:10.1099/mic.0.29239-0

Azaldegui CA, Vecchiarelli AG, Biteen JS. 2021. The emergence of phase separation as an organizing principle in bacteria. *Biophys J* **120:** 1123–1138. doi:10.1016/j.bpj.2020.09.023

Bisicchia P, Noone D, Lioliou E, Howell A, Quigley S, Jensen T, Jarmer H, Devine KM. 2007. The essential YycFG two-component system controls cell wall metabolism in *Bacillus subtilis*. *Mol Microbiol* **65:** 180–200. doi:10.1111/j.1365-2958.2007.05782.x

Bjarnadóttir TK, Fredriksson R, Höglund PJ, Gloriam DE, Lagerström MC, Schiöth HB. 2004. The human and mouse repertoire of the adhesion family of G-protein-coupled receptors. *Genomics* **84:** 23–33. doi:10.1016/j.ygeno.2003.12.004

Boeynaems S, Alberti S, Fawzi NL, Mittag T, Polymenidou M, Rousseau F, Schymkowitz J, Shorter J, Wolozin B, Van Den Bosch L, et al. 2018. Protein phase separation: a new phase in cell biology. *Trends Cell Biol* **28:** 420–435. doi:10.1016/j.tcb.2018.02.004

Brunet YR, Wang X, Rudner DZ. 2019. SweC and SweD are essential co-factors of the FtsEX–CwlO cell wall hydrolase complex in *Bacillus subtilis*. *PLoS Genet* **15:** e1008296. doi:10.1371/journal.pgen.1008296

Buske PJ, Mittal A, Pappu RV, Levin PA. 2015. An intrinsically disordered linker plays a critical role in bacterial cell division. *Semin Cell Dev Biol* **37:** 3–10. doi:10.1016/j.semcdb.2014.09.017

Carver T, Harris SR, Berriman M, Parkhill J, McQuillan JA. 2012. Artemis: an integrated platform for visualization and analysis of high-throughput sequence-based experimental data. *Bioinformatics* **28:** 464–469. doi:10.1093/bioinformatics/btr703

Cho H, Wivagg CN, Kapoor M, Barry Z, Rohs PDA, Suh H, Marto JA, Garner EC, Bernhardt TG. 2016. Bacterial cell wall biogenesis is mediated by SEDS and PBP polymerase families functioning semi-autonomously. *Nat Microbiol* **1:** 16172. doi:10.1038/nmicrobiol.2016.172

Cleverley RM, Rutter ZJ, Rismondo J, Corona F, Tsui HT, Alatawi FA, Daniel RA, Halbedel S, Massidda O, Winkler ME, et al. 2019. The cell cycle regulator GpsB functions as cytosolic adaptor for multiple cell wall enzymes. *Nat Commun* **10:** 261. doi:10.1038/s41467-018-08056-2

Dobihal GS, Brunet YR, Flores-Kim J, Rudner DZ. 2019. Homeostatic control of cell wall hydrolysis by the WalRK two-component signaling pathway in *Bacillus subtilis*. *Elife* **8:** e52088. doi:10.7554/eLife.52088

Domínguez-Cuevas P, Porcelli I, Daniel RA, Errington J. 2013. Differentiated roles for MreB-actin isologues and autolytic enzymes in *Bacillus subtilis* morphogenesis. *Mol Microbiol* **89:** 1084–1098. doi:10.1111/mmi.12335

Doyle RJ, Koch AL. 1987. The functions of autolysins in the growth and division of *Bacillus subtilis*. *Crit Rev Microbiol* **15:** 169–222. doi:10.3109/10408418709104457

Drozdetskiy A, Cole C, Procter J, Barton GJ. 2015. JPred4: a protein secondary structure prediction server. *Nucleic Acids Res* **43:** W389–W394. doi:10.1093/nar/gkv332

Du S, Park KT, Lutkenhaus J. 2015. Oligomerization of FtsZ converts the FtsZ tail motif (conserved carboxy-terminal peptide) into a multivalent ligand with high avidity for partners ZipA and SlmA. *Mol Microbiol* **95:** 173–188. doi:10.1111/mmi.12854

Ellermeier CD, Losick R. 2006. Evidence for a novel protease governing regulated intramembrane proteolysis and resistance to antimicrobial peptides in *Bacillus subtilis*. *Genes Dev* **20:** 1911–1922. doi:10.1101/gad.1440606

Fujita M, Sadaie Y. 1998. Promoter selectivity of the *Bacillus subtilis* RNA polymerase σ^A and σ^H holoenzymes. *J Biochem* **124:** 89–97. doi:10.1093/oxfordjournals.jbchem.a022102

Gardner KA, Moore DA, Erickson HP. 2013. The C-terminal linker of *Escherichia coli* FtsZ functions as an intrinsically disordered peptide. *Mol Microbiol* **89:** 264–275. doi:10.1111/mmi.12279

Gibson DG. 2011. Enzymatic assembly of overlapping DNA fragments. *Methods Enzymol* **498:** 349–361. doi:10.1016/B978-0-12-385120-8.00015-2

Goffin C, Ghuysen JM. 1998. Multimodular penicillin-binding proteins: an enigmatic family of orthologs and paralogs. *Microbiol Mol Biol Rev* **62:** 1079–1093. doi:10.1128/MMBR.62.4.1079-1093.1998

Gordon WR, Zimmerman B, He L, Miles LJ, Huang J, Tiyanont K, McArthur DG, Aster JC, Perrimon N, Loparo JJ, et al. 2015. Mechanical allostery: evidence for a force requirement in the proteolytic activation of Notch. *Dev Cell* **33:** 729–736. doi:10.1016/j.devcel.2015.05.004

Griffith KL, Grossman AD. 2008. Inducible protein degradation in *Bacillus subtilis* using heterologous peptide tags and adaptor proteins to target substrates to the protease ClpXP. *Mol Microbiol* **70:** 1012–1025.

Harami GM, Kovács ZJ, Pancsa R, Pálinkáas J, Baráth V, Tárnok K, Málnási-Csizmadia A, Kovács M. 2020. Phase separation by ssDNA binding protein controlled via protein-protein and protein-DNA interactions. *Proc Natl Acad Sci* **117:** 26206–26217. doi:10.1073/pnas.2000761117

Harwood CR, Cutting SM. 1990. *Molecular biological methods for bacillus*. Wiley, New York.

Hashimoto M, Ooiwa S, Sekiguchi J. 2012. Synthetic lethality of the *lytE cwlO* genotype in *Bacillus subtilis* is caused by lack of D,L-endopeptidase activity at the lateral cell wall. *J Bacteriol* **194:** 796–803. doi:10.1128/JB.05569-11

Hastie JL, Williams KB, Ellermeier CD. 2013. The activity of σ^V, an extracytoplasmic function σ factor of *Bacillus subtilis*, is controlled by regulated proteolysis of the anti-σ factor RsiV. *J Bacteriol* **195:** 3135–3144. doi:10.1128/JB.00292-13

Heinrich J, Lundén T, Kontinen VP, Wiegert T. 2008. The *Bacillus subtilis* ABC transporter EcsAB influences intramembrane proteolysis through RasP. *Microbiology (Reading)* **154:** 1989–1997. doi:10.1099/mic.0.2008/018648-0

Hizukuri Y, Oda T, Tabata S, Tamura-Kawakami K, Oi R, Sato M, Takagi J, Akiyama Y, Nogi T. 2014. A structure-based model

of substrate discrimination by a noncanonical PDZ tandem in the intramembrane-cleaving protease RseP. *Structure* **22:** 326–336. doi:10.1016/j.str.2013.12.003

Ho TD, Ellermeier CD. 2012. Extra cytoplasmic function σ factor activation. *Curr Opin Microbiol* **15:** 182–188. doi:10.1016/j.mib.2012.01.001

Ho TD, Ellermeier CD. 2019. Activation of the extracytoplasmic function σ factor σ^V by lysozyme. *Mol Microbiol* **112:** 410–419. doi:10.1111/mmi.14348

Holmes JA, Follett SE, Wang H, Meadows CP, Varga K, Bowman GR. 2016. *Caulobacter* PopZ forms an intrinsically disordered hub in organizing bacterial cell poles. *Proc Natl Acad Sci* **113:** 12490–12495. doi:10.1073/pnas.1602380113

Johnson CM, Grossman AD. 2014. Identification of host genes that affect acquisition of an integrative and conjugative element in *Bacillus subtilis*. *Mol Microbiol* **93:** 911–927. doi:10.1111/mmi.12704

Jumper J, Evans R, Pritzel A, Green T, Figurnov M, Ronneberger O, Tunyasuvunakool K, Bates R, Žídek A, Potapenko A, et al. 2021. Highly accurate protein structure prediction with AlphaFold. *Nature* **596:** 583–589. doi:10.1038/s41586-021-03819-2

Kahel-Raifer H, Jindou S, Bahari L, Nataf Y, Shoham Y, Bayer EA, Borovok I, Lamed R. 2010. The unique set of putative membrane-associated anti-σ factors in *Clostridium thermocellum* suggests a novel extracellular carbohydrate-sensing mechanism involved in gene regulation. *FEMS Microbiol Lett* **308:** 84–93. doi:10.1111/j.1574-6968.2010.01997.x

Kanehara K, Ito K, Akiyama Y. 2002. Yael (EcfE) activates the σ^E pathway of stress response through a site-2 cleavage of anti-σ^E, RseA. *Genes Dev* **16:** 2147–2155. doi:10.1101/gad.1002302

Kopan R, Ilagan MX. 2009. The canonical Notch signaling pathway: unfolding the activation mechanism. *Cell* **137:** 216–233. doi:10.1016/j.cell.2009.03.045

Kroos L, Akiyama Y. 2013. Biochemical and structural insights into intramembrane metalloprotease mechanisms. *Biochim Biophys Acta* **1828:** 2873–2885. doi:10.1016/j.bbamem.2013.03.032

Lai GC, Cho H, Bernhardt TG. 2017. The mecillinam resistome reveals a role for peptidoglycan endopeptidases in stimulating cell wall synthesis in *Escherichia coli*. *PLoS Genet* **13:** e1006934. doi:10.1371/journal.pgen.1006934

Langenhan T, Aust G, Hamann J. 2013. Sticky signaling—adhesion class G protein-coupled receptors take the stage. *Sci Signal* **6:** re3. doi:10.1126/scisignal.2003825

Lasker K, von Diezmann L, Zhou X, Ahrens DG, Mann TH, Moerner WE, Shapiro L. 2020. Selective sequestration of signalling proteins in a membraneless organelle reinforces the spatial regulation of asymmetry in *Caulobacter crescentus*. *Nat Microbiol* **5:** 418–429. doi:10.1038/s41564-019-0647-7

Levin PA, Kurtser IG, Grossman AD. 1999. Identification and characterization of a negative regulator of FtsZ ring formation in *Bacillus subtilis*. *Proc Natl Acad Sci* **96:** 9642–9647. doi:10.1073/pnas.96.17.9642

Liebscher I, Schön J, Petersen SC, Fischer L, Auerbach N, Demberg LM, Mogha A, Cöster M, Simon KU, Rothemund S, et al. 2014. A tethered agonist within the ectodomain activates the adhesion G protein-coupled receptors GPR126 and GPR133. *Cell Rep* **9:** 2018–2026. doi:10.1016/j.celrep.2014.11.036

Liu TY, Chu SH, Hu YN, Wang JJ, Shaw GC. 2017. Genetic evidence that multiple proteases are involved in modulation of heat-induced activation of the σ factor SigI in *Bacillus subtilis*. *FEMS Microbiol Lett* **364:** fnx054. doi:10.1093/femsle/fnx054

Meeske AJ, Sham LT, Kimsey H, Koo BM, Gross CA, Bernhardt TG, Rudner DZ. 2015. Murj and a novel lipid II flippase are required for cell wall biogenesis in *Bacillus subtilis*. *Proc Natl Acad Sci* **112:** 6437–6442. doi:10.1073/pnas.1504967112

Meeske AJ, Riley EP, Robins WP, Uehara T, Mekalanos JJ, Kahne D, Walker S, Kruse AC, Bernhardt TG, Rudner DZ. 2016. SEDS proteins are a widespread family of bacterial cell wall polymerases. *Nature* **537:** 634–638. doi:10.1038/nature19331

Meisner J, Montero Llopis P, Sham LT, Garner E, Bernhardt TG, Rudner DZ. 2013. FtsEX is required for CwlO peptidoglycan hydrolase activity during cell wall elongation in *Bacillus subtilis*. *Mol Microbiol* **89:** 1069–1083. doi:10.1111/mmi.12330

Miller JH. 1972. *Experiments in molecular genetics*. Cold Spring Harbor Laboratory, Cold Spring Harbor, NY.

Muñoz-Gutiérrez I, Ortiz de Ora L, Rozman Grinberg I, Garty Y, Bayer EA, Shoham Y, Lamed R, Borovok I. 2016. Decoding biomass-sensing regulons of *Clostridium thermocellum* alternative σ^I factors in a heterologous *Bacillus subtilis* host system. *PLoS One* **11:** e0146316. doi:10.1371/journal.pone.0146316

Musse AA, Meloty-Kapella L, Weinmaster G. 2012. Notch ligand endocytosis: mechanistic basis of signaling activity. *Semin Cell Dev Biol* **23:** 429–436. doi:10.1016/j.semcdb.2012.01.011

Nataf Y, Bahari L, Kahel-Raifer H, Borovok I, Lamed R, Bayer EA, Sonenshein AL, Shoham Y. 2010. *Clostridium thermocellum* cellulosomal genes are regulated by extracytoplasmic polysaccharides via alternative σ factors. *Proc Natl Acad Sci* **107:** 18646–18651. doi:10.1073/pnas.1012175107

Nichols JT, Miyamoto A, Olsen SL, D'Souza B, Yao C, Weinmaster G. 2007. DSL ligand endocytosis physically dissociates Notch1 heterodimers before activating proteolysis can occur. *J Cell Biol* **176:** 445–458. doi:10.1083/jcb.200609014

Oldfield CJ, Dunker AK. 2014. Intrinsically disordered proteins and intrinsically disordered protein regions. *Annu Rev Biochem* **83:** 553–584. doi:10.1146/annurev-biochem-072711-164947

Ortiz de Ora L, Lamed R, Liu YJ, Xu J, Cui Q, Feng Y, Shoham Y, Bayer EA, Muñoz-Gutiérrez I. 2018. Regulation of biomass degradation by alternative σ factors in cellulolytic clostridia. *Sci Rep* **8:** 11036. doi:10.1038/s41598-018-29245-5

Paradis-Bleau C, Markovski M, Uehara T, Lupoli TJ, Walker S, Kahne DE, Bernhardt TG. 2010. Lipoprotein cofactors located in the outer membrane activate bacterial cell wall polymerases. *Cell* **143:** 1110–1120. doi:10.1016/j.cell.2010.11.037

Pasquina-Lemonche L, Burns J, Turner RD, Kumar S, Tank R, Mullin N, Wilson JS, Chakrabarti B, Bullough PA, Foster SJ, et al. 2020. The architecture of the Gram-positive bacterial cell wall. *Nature* **582:** 294–297. doi:10.1038/s41586-020-2236-6

Patel Y, Zhao H, Helmann JD. 2020. A regulatory pathway that selectively up-regulates elongasome function in the absence of class A PBPs. *Elife* **9:** e57902. doi:10.7554/eLife.57902

Qiao Y, Lebar MD, Schirner K, Schaefer K, Tsukamoto H, Kahne D, Walker S. 2014. Detection of lipid-linked peptidoglycan precursors by exploiting an unexpected transpeptidase reaction. *J Am Chem Soc* **136:** 14678–14681. doi:10.1021/ja508147s

Qiao Y, Srisuknimit V, Rubino F, Schaefer K, Ruiz N, Walker S, Kahne D. 2017. Lipid II overproduction allows direct assay of transpeptidase inhibition by β-lactams. *Nat Chem Biol* **13:** 793–798. doi:10.1038/nchembio.2388

Rohs PDA, Bernhardt TG. 2021. Growth and division of the peptidoglycan matrix. *Annu Rev Microbiol* **75:** 315–336. doi:10.1146/annurev-micro-020518-120056

Rudner DZ, Losick R. 2002. A sporulation membrane protein tethers the pro-σ^K processing enzyme to its inhibitor and dictates its subcellular localization. *Genes Dev* **16:** 1007–1018. doi:10.1101/gad.977702

Rudner DZ, Fawcett P, Losick R. 1999. A family of membrane-embedded metalloproteases involved in regulated proteolysis of membrane-associated transcription factors. *Proc Natl Acad Sci* **96:** 14765–14770. doi:10.1073/pnas.96.26.14765

Salzberg LI, Powell L, Hokamp K, Botella E, Noone D, Devine KM. 2013. The WalRK (YycFG) and σ^I RsgI regulators cooperate to control CwlO and LytE expression in exponentially growing and stressed *Bacillus subtilis* cells. *Mol Microbiol* **87:** 180–195. doi:10.1111/mmi.12092

Schneider JS, Glickman MS. 2013. Function of site-2 proteases in bacteria and bacterial pathogens. *Biochim Biophys Acta* **1828:** 2808–2814. doi:10.1016/j.bbamem.2013.04.019

Schöbel S, Zellmeier S, Schumann W, Wiegert T. 2004. The *Bacillus subtilis* σW anti-σ factor RsiW is degraded by intramembrane proteolysis through YluC. *Mol Microbiol* **52:** 1091–1105. doi:10.1111/j.1365-2958.2004.04031.x

Sjodt M, Rohs PDA, Gilman MSA, Erlandson SC, Zheng S, Green AG, Brock KP, Taguchi A, Kahne D, Walker S, et al. 2020. Structural coordination of polymerization and crosslinking by a SEDS–bPBP peptidoglycan synthase complex. *Nat Microbiol* **5:** 813–820. doi:10.1038/s41564-020-0687-z

Sklar JG, Makinoshima H, Schneider JS, Glickman MS. 2010. M. tuberculosis intramembrane protease Rip1 controls transcription through three anti-σ factor substrates. *Mol Microbiol* **77:** 605–617. doi:10.1111/j.1365-2958.2010.07232.x

Soppa J, Kobayashi K, Noirot-Gros MF, Oesterhelt D, Ehrlich SD, Dervyn E, Ogasawara N, Moriya S. 2002. Discovery of two novel families of proteins that are proposed to interact with prokaryotic SMC proteins, and characterization of the *Bacillus subtilis* family members ScpA and ScpB. *Mol Microbiol* **45:** 59–71. doi:10.1046/j.1365-2958.2002.03012.x

Sprinzak D, Blacklow SC. 2021. Biophysics of Notch signaling. *Annu Rev Biophys* **50:** 157–189. doi:10.1146/annurev-biophys-101920-082204

Stoveken HM, Hajduczok AG, Xu L, Tall GG. 2015. Adhesion G protein-coupled receptors are activated by exposure of a cryptic tethered agonist. *Proc Natl Acad Sci* **112:** 6194–6199. doi:10.1073/pnas.1421785112

Taguchi A, Welsh MA, Marmont LS, Lee W, Sjodt M, Kruse AC, Kahne D, Bernhardt TG, Walker S. 2019. Ftsw is a peptidoglycan polymerase that is functional only in complex with its cognate penicillin-binding protein. *Nat Microbiol* **4:** 587–594. doi:10.1038/s41564-018-0345-x

Tseng CL, Shaw GC. 2008. Genetic evidence for the actin homolog gene mreBH and the bacitracin resistance gene bcrC as targets of the alternative σ factor SigI of *Bacillus subtilis*. *J Bacteriol* **190:** 1561–1567. doi:10.1128/JB.01497-07

Tseng CL, Chen JT, Lin JH, Huang WZ, Shaw GC. 2011. Genetic evidence for involvement of the alternative σ factor SigI in controlling expression of the cell wall hydrolase gene lytE and contribution of LytE to heat survival of *Bacillus subtilis*. *Arch Microbiol* **193:** 677–685. doi:10.1007/s00203-011-0710-0

Typas A, Banzhaf M, van den Berg van Saparoea B, Verheul J, Biboy J, Nichols RJ, Zietek M, Beilharz K, Kannenberg K, von Rechenberg M, et al. 2010. Regulation of peptidoglycan synthesis by outer-membrane proteins. *Cell* **143:** 1097–1109. doi:10.1016/j.cell.2010.11.038

Typas A, Banzhaf M, Gross CA, Vollmer W. 2012. From the regulation of peptidoglycan synthesis to bacterial growth and morphology. *Nat Rev Microbiol* **10:** 123–136. doi:10.1038/nrmicro2677

Uehara T, Bernhardt TG. 2011. More than just lysins: peptidoglycan hydrolases tailor the cell wall. *Curr Opin Microbiol* **14:** 698–703. doi:10.1016/j.mib.2011.10.003

van Opijnen T, Bodi KL, Camilli A. 2009. Tn-seq: high-throughput parallel sequencing for fitness and genetic interaction studies in microorganisms. *Nat Methods* **6:** 767–772. doi:10.1038/nmeth.1377

Vigouroux A, Cordier B, Aristov A, Alvarez L, Ozbaykal G, Chaze T, Oldewurtel ER, Matondo M, Cava F, Bikard D, et al. 2020. Class-A penicillin binding proteins do not contribute to cell shape but repair cell-wall defects. *Elife* **9:** e51998. doi:10.7554/eLife.51998

Wang X, Le TB, Lajoie BR, Dekker J, Laub MT, Rudner DZ. 2015. Condensin promotes the juxtaposition of DNA flanking its loading site in *Bacillus subtilis*. *Genes Dev* **29:** 1661–1675. doi:10.1101/gad.265876.115

Weidel W, Pelzer H. 1964. Bagshaped macromolecules—a new outlook on bacterial cell walls. *Adv Enzymol Relat Subj Biochem* **26:** 193–232.

Welsh MA, Taguchi A, Schaefer K, Van Tyne D, Lebreton F, Gilmore MS, Kahne D, Walker S. 2017. Identification of a functionally unique family of penicillin-binding proteins. *J Am Chem Soc* **139:** 17727–17730. doi:10.1021/jacs.7b10170

Wright PE, Dyson HJ. 2015. Intrinsically disordered proteins in cellular signalling and regulation. *Nat Rev Mol Cell Biol* **16:** 18–29. doi:10.1038/nrm3920

Yaniv O, Morag E, Borovok I, Bayer EA, Lamed R, Frolow F, Shimon LJ. 2013. Structure of a family 3a carbohydrate-binding module from the cellulosomal scaffoldin CipA of *Clostridium thermocellum* with flanking linkers: implications for cellulosome structure. *Acta Crystallogr Sect F Struct Biol Cryst Commun* **69:** 733–737. doi:10.1107/S174430911301614X

Youngman PJ, Perkins JB, Losick R. 1983. Genetic transposition and insertional mutagenesis in *Bacillus subtilis* with streptococcus faecalis transposon Tn917. *Proc Natl Acad Sci* **80:** 2305–2309. doi:10.1073/pnas.80.8.2305

Zellmeier S, Schumann W, Wiegert T. 2006. Involvement of Clp protease activity in modulating the *Bacillus subtilis* σ^W stress response. *Mol Microbiol* **61:** 1569–1582. doi:10.1111/j.1365-2958.2006.05323.x

Zuber U, Drzewiecki K, Hecker M. 2001. Putative σ factor SigI (YkoZ) of *Bacillus subtilis* is induced by heat shock. *J Bacteriol* **183:** 1472–1475. doi:10.1128/JB.183.4.1472-1475.2001